

# A flow-through infusion calorimeter for measuring muscle energetics: design and performance

Andrew J. Taberner, Callum M. Johnston, Toan Pham, June-Chiew Han, Riaz Uddin, Denis S. Loiselle, Bryan P. Ruddy, and Poul M. F. Nielsen.

**Abstract**— The heat produced during muscle contraction arises from distinct underlying cellular processes. While current calorimeters can measure total muscle heat production, none can allow accurate titration and infusion of chemical drugs to probe the thermodynamic mechanisms that underlie various heart diseases. We have constructed a calorimeter that incorporates an infusion system for exposing muscle samples to time-varying concentrations of pharmacological agents. The design of the instrument is informed by the development and use of analytical lumped parameter and finite element models. This new infusion calorimeter uses thermopile-based heat sensors to achieve a noise-equivalent power of  $2.6 \text{ nW}\cdot\text{Hz}^{-1/2}$ , and a signal to noise ratio of up to approximately 1700. We report on the modelling and optimization techniques that were used to inform our design. We characterize the instrument’s performance, and demonstrate its utility by exposing muscle to pharmacological interventions that mimic two cardiac disease conditions: acute force impairment and dynamic contracture.

**Index Terms**— calorimeter, thermopile, muscle, energetics

## I. INTRODUCTION

MUSCLE is a thermodynamic machine that converts chemical enthalpy into mechanical work. The efficiency with which it does so is modest ( $\sim 15\%$ ) [1-3]; the majority of the change in enthalpy is liberated as heat. The heat produced by muscle tissues arises from the various cellular processes that underlie muscle function. These processes are involved in general maintenance of the muscle tissues (‘basal heat’), activating the muscle to a state where it is ready to produce force (‘activation heat’) and the production of force and work (‘cross-bridge heat’). Each of these processes can be perturbed by physiological and pharmacological interventions, and can become dysfunctional in disease.

Submitted for review, June 28 2017. This work was supported by the Marsden Fund, administered by the Royal Society of New Zealand (#UOA1108), the Medical Technologies Centre of Research Excellence, funded by the Tertiary Education Commission of New Zealand, and by National Heart Foundation (NZ) Project Grant 1601.

All authors were with the Auckland Bioengineering Institute, University of Auckland, Auckland, New Zealand, at the time this work was performed. A. Taberner, B. Ruddy, and P. Nielsen are also with the Department of Engineering Science, University of Auckland. (email: [a.taberner@auckland.ac.nz](mailto:a.taberner@auckland.ac.nz)). T. Pham and D. Loiselle are also with the Department of Physiology, University of Auckland. C. Johnston is now with the Institute for Experimental Cardiovascular Medicine, Albert-Ludwigs University, Freiburg, Germany.

For more than a century, measurements of heat production have provided useful insight into the characteristics of muscle tissue, in health and disease [5]. A variety of calorimeters have been constructed to measure the heat production of muscle samples maintained by a supply of oxygen and nutrients [3, 6, 7]. However, it is only relatively recently that flow-through calorimeters have been constructed in a form that allows concurrent measurements of heat and force [1, 4].

Despite recent advances in the design of calorimeters for the study of cardiac energetics, no previously reported calorimeters have allowed muscle samples to be systematically exposed to pharmacological interventions that mimic many cardiac disease conditions. The development of this capability would allow the use of system identification techniques to probe, individually, the processes that underlie muscle contraction, and thus advance our understanding of the cellular mechanisms behind cardiac failure.

To address this deficit, we have recently constructed a new flow-through infusion calorimeter that allows us to examine the energetic processes within cardiac muscle samples by perturbing the chemical composition of the fluids to which they are exposed [8]. Our calorimeter is unique in allowing muscle heat rate to be measured simultaneously with force and shortening, during systematic pharmacological interventions.

Here, we report in detail on its design and construction, and quantify its performance. We develop equations and models that describe the physics of the heat measurement technique, predict the performance of different design options, and thereby identify the design of a suitable device. The new flow-through infusion calorimeter successfully allows us to quantify the energetic processes within cardiac muscle samples by perturbing the chemical composition of the fluids to which they are exposed. This is demonstrated in a series of experiments in which (i) we sequentially inhibit and engage the contractile processes in a sample of cardiac tissue, by chemical intervention, and (ii) we measure the maximum total heat production of a muscle as it transitions into chemically-induced contracture. These two experiments mimic cardiac disease states where the molecular force-producing elements are impaired or challenged.

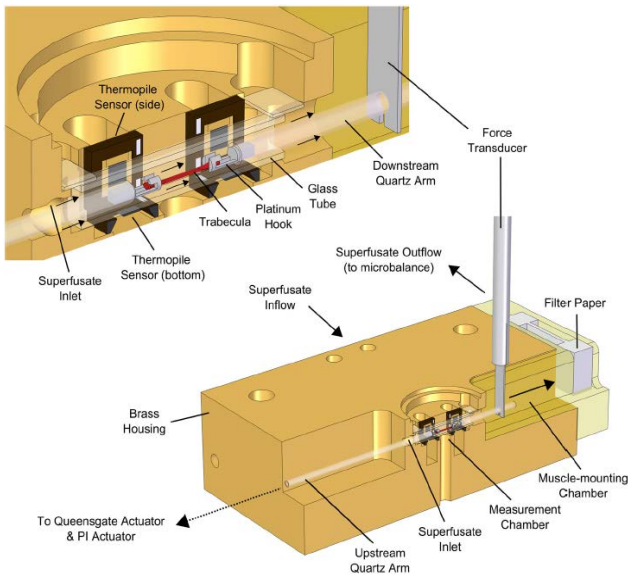


**Fig. 1.** Cutaway views of a flow-through calorimeter system, reproduced from [4], with permission. In this design, heat is transported from the muscle (trabecula) by flowing fluid (superfusate) to an enclosing glass tube, then conducted through an air layer, to an adjacent infra-red thermopile detector.

## II. DESIGN CONSIDERATIONS

### A. Measurement Principle

Our muscle calorimeter continues the flow-through differential approach that has been used successfully in previous devices [1, 4, 7, 9]. In these instruments, the rate of heat production of a muscle sample is inferred from the temperature increase it imparts to a fluid flowing along its length. A muscle sample is advanced into the center of a ‘measurement chamber’ (Fig. 1.) comprising a 1 mm square cross section borosilicate glass tube filled with flowing oxygenated superfusate. Platinum hooks secure the ends of the muscle to a linear positioner (upstream) and force transducer (downstream) via quartz tubes. Temperature sensors are placed in proximity to the external surface of the glass tube, upstream and downstream of the muscle. The muscle heat rate is inferred from the difference between the temperature estimates gathered at these two locations.

Others have developed custom thin-film thermopile temperature sensors for use in microfluidic drug reaction calorimeters [10, 11]. These sensors can provide resolutions in the 10 nW range, but suffer from the fragility of the substrates on which they are constructed and are not conducive to the open-ended configuration required for this application. We have previously reported on our own novel use of thin-film thermopiles (designed for use in infrared thermometers, but used by us as conduction-mode temperature sensors [6]), and on our experimental development of vapour-pressure temperature sensors [12, 13]. While both of these techniques have proven feasible and useful, they are limited by the fragility and inferior reliability of the sensors.

In contrast, thermoelectric modules (TEMs; often referred to as ‘Peltier coolers’ or ‘thermoelectric heat pumps’) are a

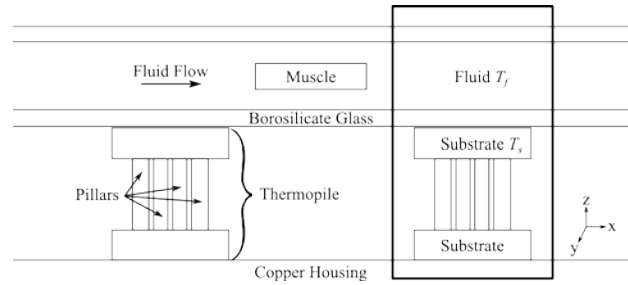


**Fig. 2.** Schematic of the calorimeter system. The lumped parameter model examines the section of the calorimeter contained within the box.

robust and readily-available alternative form of thermopile. These sensors have found use in balance calorimeters for RF power loss measurement [14, 15], and in isothermal titration calorimeters for drug discovery [16, 17]. In this work, we report on our recent use of TEMs as temperature sensors in our flow-through infusion calorimeter.

TEMs are thermopiles comprising alternating pillars of two thermocouple materials (typically alloys of bismuth telluride) thermally arranged in parallel, but electrically connected in series. While they are primarily intended to actively pump heat, they can also be used as sensors that provide a voltage in proportion to the temperature difference developed between their two faces. By bonding one face of a TEM to the surface of the glass tube, and its other surface to a reference material (Fig. 2, copper housing), the temperature difference between the glass tube and the reference material can be inferred from the thermopile voltage. The difference between the upstream and downstream sensor voltage signals is used to infer muscle heat output, with the added advantage that common-mode noise is removed.

TEMs of a variety of dimensions are readily available. In order to select thermopiles with dimensions and materials suitable for use in a flow-through calorimeter we turned to mathematical modelling methods. Others have developed models of heat flow in TEMs being used in applications for power generation [18, 19]. However, in this application, no electrical power is demanded by the amplifying electronics, and the flow-through configuration of our device demands consideration of additional physics. Thus, we first developed a lumped parameter model of our proposed design to narrow our selection of thermopile devices, and then used finite element methods to determine an appropriate final selection and arrangement in a calorimeter. Our goal was to determine a calorimeter design that provided a high signal to noise ratio (SNR) but was also relatively straightforward to assemble, and robust.

### B. Analytical Modelling

The voltage generated by a thermopile sensor arises from the temperature difference developed between its faces, and is proportional to the number of thermocouple pillar pairs in the array. The total *thermal* resistance of the thermopile should be high compared to the thermal resistance between the thermopile and the heat source, in order to maximize the temperature gradient across the sensor, and thus the signal.

The thermal resistances of the pillars add in parallel – increasing their number or area decreases the total thermal resistance. At the same time, the electrical noise generated in the thermopile is proportional to the square root of their total series *electrical* resistance, which increases with number of pillars and decreases with their cross-sectional area.

A lumped parameter analytical model was thus used to investigate how these thermopile parameters together determine the sensitivity and noise parameters of the proposed design, and its resulting SNR. The model examined the heat flow path between the fluid and the copper housing across the downstream thermopile as shown in Fig. 2, and the corresponding temperature differences that arise. A steady state model with adiabatic boundaries was considered, with heat permitted to flow into this region at rate  $\dot{Q}$ . A portion of this heat is conducted through the thermopile, while the remainder is transported from the fluid outlet. The thermopile substrate's thermal conductivity was at least 20-fold higher than the glass and fluid, and was thus modelled as a thermal conductor of infinite conductivity; the conduction of heat in the  $x$  direction, except via the substrate, was not considered in this model. The fluid temperature was assumed to be constant in  $y$  and  $z$  and the copper housing was taken to be a perfect heat sink. All temperatures are reported relative to the housing.

The temperature difference between the fluid and the substrate at any point may be found by performing a heat balance analysis on an infinitesimally thin section (in the  $x$  direction) of the fluid. The resulting temperature profile is given by

$$T_f(x) - T_s = (T_f(0) - T_s) \exp\left(\frac{-x}{\dot{m}C_p X R_g}\right), \quad (1)$$

where  $T_f$  and  $T_s$  are the fluid and substrate temperature, respectively,  $x$  is the distance from the left-hand end of the thermopile,  $\dot{m}$  is the fluid mass flow rate,  $C_p$  is the fluid specific heat capacity,  $X$  is the total length and  $R_g$  is the absolute thermal resistance of the glass. The rate of energy entering the fluid volume is equal to the rate of energy output of the muscle, i.e.,  $\dot{m}C_p T_f(0) = \dot{Q}$ .

The substrate temperature may be found by considering a

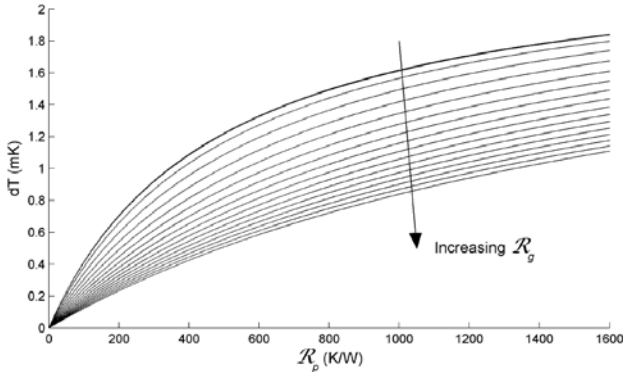


**Fig. 3.** Predicted temperature difference across a thermopile depending upon the pillar thermal resistance ( $R_p$ ) and the glass thermal resistance ( $R_g$ ).  $R_g$  varies linearly between 0 K/W and 500 K/W. The temperature difference was calculated for fluid flow rate of 0.5  $\mu$ l/s and a muscle heat output of 5  $\mu$ W.

heat balance across the total fluid volume above the thermopile. Solving for the substrate temperature gives

$$T_s = \dot{Q} R_p \left( \frac{\varepsilon}{1 + \dot{m} C_p R_p \varepsilon} \right), \quad (2)$$

where  $R_p$  is the absolute thermal resistance of the pillars and

$$\varepsilon = 1 - \exp\left(\frac{-1}{\dot{m} C_p R_g}\right). \quad (3)$$

$\varepsilon$  is the *heat exchanger effectiveness* and reflects the efficiency of heat transfer between the fluid and the substrate if the substrate is assumed to be a heat sink, i.e.  $R_p$  is zero.

Given the model assumptions, the temperature difference across the pillars ( $dT$ ) is equal to the substrate temperature. The dependence of  $dT$  on the absolute thermal resistance of the pillars and the glass is shown in Fig. 3. As expected, the temperature difference is maximized by using a system with a high combined pillar thermal resistance and a low glass thermal resistance. However, we must also take into account the effect of these design choices on the corresponding electrical properties of the sensor.

The voltage signal arising in the sensor may be estimated by multiplying the temperature difference by the number of thermocouples ( $n$ ) and their Seebeck coefficient ( $S$ ). The dominant noise source in thermocouples is typically Johnson noise. Thus, the SNR may be found by dividing the expected voltage difference by the Johnson noise, such that

$$\text{SNR} = \frac{n S dT}{\sqrt{4 k_B T R_e \Delta f}}, \quad (4)$$

where  $k_B$  is the Boltzmann constant,  $T$  is the absolute temperature,  $R_e$  is the electrical resistance and  $\Delta f$  is the measurement bandwidth.

Combining (2) and (4), in addition to the electrical resistance as a function of the number of thermocouples, the ratio of pillar area ( $A_p$ ) to height ( $Z_p$ ) and the pillar's electrical resistivity ( $\rho$ ) gives

$$\text{SNR} = \frac{\dot{Q} S \sqrt{R_p}}{\sqrt{16 k_B \kappa_p \rho \Delta f T}} \cdot \left[ \frac{\varepsilon}{1 + \dot{m} C_p R_p \varepsilon} \right], \quad (5)$$

where  $\kappa_p$  is the thermal conductivity of the pillars.

The dependence of the SNR on the number of pillars and their form factor is displayed in Fig. 4. For a sensor of given length  $X$ , the maximum SNR is independent of the pillar

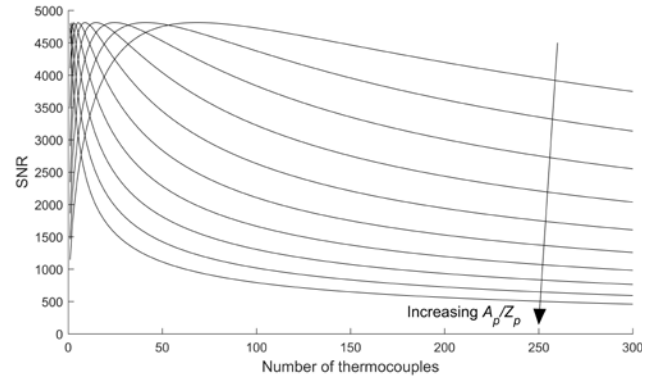


**Fig. 4.** Predicted signal-to-noise ratio (SNR) across a thermopile depending upon the number of thermocouples and ratio of pillar area ( $A_p$ ) to pillar height ( $Z_p$ ).  $A_p/Z_p$  varies logarithmically from 10 nm to 1000 nm. The thermal resistance of the glass was 100 K/W, the fluid flow rate was 0.5  $\mu$ l/s, the muscle heat output was 5  $\mu$ W and the bandwidth was 5 Hz.

**Fig. 5.** Predicted signal-to-noise ratio (SNR) for a range of thermal resistances of the pillars ( $R_p$ ) and combinations of mass flow rate ( $\dot{m}$ ) and specific heat capacity of the fluid ( $C_p$ ).  $R_p$  varies logarithmically from 10 K/W to  $10^4$  K/W. The thermal resistance of the glass was 100 K/W, the muscle heat output was  $5 \mu\text{W}$  and the bandwidth was 5 Hz.

geometry. The maxima occur at the same pillar thermal resistances; i.e. there is an ideal thermal resistance for any combination of volumetric flow rate and specific heat capacity of the fluid. The thermal resistance at which the maximum occurs depends on  $R_g$  but the effect is minimal over a relatively wide range.  $R_g$  can be up to 30 % of  $R_p$  with only a 5 % change in the value of  $R_p$  at which the maximum SNR occurs. The dependence of the SNR on the product of the mass flow rate and the specific heat capacity for a range of pillar thermal resistances is shown in Fig. 5.

Equation (4) can be rewritten as

$$\text{SNR} = \frac{\dot{Q}}{2} \cdot \frac{\sqrt{ZT}}{\sqrt{4k_B\Delta fT^2G_p}} \cdot \left[ \frac{\epsilon}{1 + \dot{m}C_pR_p\epsilon} \right], \quad (5)$$

where  $G_p$  is the thermal conductance of the pillar layer and  $ZT$  is the dimensionless thermoelectric figure of merit often used in temperature control literature [20].  $Z$  is the ratio of the square of the Seebeck coefficient to the product of the resistivity and the thermal conductivity, and is closely linked to the efficiency of thermoelectric devices. A more efficient thermoelectric material therefore will also be a better power sensor.

The denominator of the second term in (5) is the phonon noise, a result of the random movement of energy carriers between the sensor and its environment [21, 22]. The

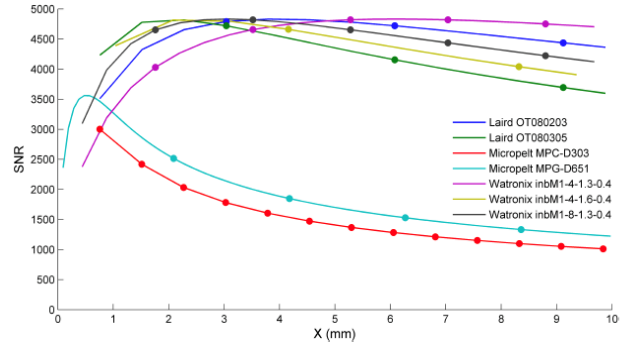


**Fig. 6.** Predicted signal-to-noise ratio (SNR) depending on the thermopile design used and the total module length. Filled symbols indicate currently-available module lengths. The fluid flow rate was  $0.5 \mu\text{l/s}$ , the muscle heat output was  $5 \mu\text{W}$  and the measurement bandwidth was 5 Hz.

movement occurs even when the sensor is in equilibrium with the environment, thus reflecting the absolute limit on thermal power measurement.

Using this model, a range of commercially-available thermoelectric module families was assessed. Table I lists the properties of the sensors, all of which use bismuth telluride thermocouples. Bismuth telluride is commonly used for its high thermoelectric figure of merit ( $ZT = 0.80$  at  $25^\circ\text{C}$ ).

The SNR of these various sensor designs is shown in Fig. 6 as a function of the module length. While the sensors themselves are available only in discrete lengths (filled symbols), this approach allows us to identify for each family an ‘optimal’ length beyond which the SNR is not enhanced by the use of additional thermopile pillars.

Fig. 6 indicates that the Laird and Watronix thermopile families provide similar peak SNR. These thermopiles have few, tall thermocouple pillars, while the Micropelt sensors are of a radically different design, comprising many, very short pillars, that may be more suitable for other applications such as energy harvesting. The results show that the peak SNR is obtained at a thermopile length of between 2 mm and 3 mm.

### C. Finite Element Modelling

The analytical model developed in Section IIB provides useful design guidance, but makes a number of simplifying assumptions that require further consideration. In particular,

TABLE I. THERMOPILE PROPERTIES

Manufacturer	Module	Dimensions $X$ (mm) • $Y$ (mm) • $Z$ (mm)			Number of Thermocouples	Resistance ( $\Omega$ )
		Base	Top	Pillar		
Laird	OT08-0203	3.4 • 3.4 • 0.50	3.4 • 1.61 • 0.50	0.44 • 0.44 • 1.45	4	0.55
	OT08-0305	4.9 • 4.9 • 0.50	4.9 • 4.9 • 0.50	0.44 • 0.44 • 1.45	10	1.43
Micropelt	MPC-D303	0.83 • 2.42 • 0.53	0.83 • 1.18 • 0.53	0.69 • 0.07 • 0.04	4	0.3
	MPG-D651	2.50 • 3.35 • 0.53	2.50 • 2.50 • 0.53	0.04 • 0.04 • 0.04	286	185
Watronix	inbM1-4-1.3-0.4	2.26 • 2.08 • 0.50	2.08 • 1.14 • 0.50	0.26 • 0.26 • 1.35	4	2.7
	inbM1-4-1.6-1.3	4.18 • 3.34 • 0.50	4.18 • 2.18 • 0.50	0.70 • 0.70 • 1.65	4	0.39
	inbM1-8-1.3-0.4	2.04 • 3.22 • 0.50	2.04 • 2.04 • 0.50	0.26 • 0.26 • 1.35	8	2.97

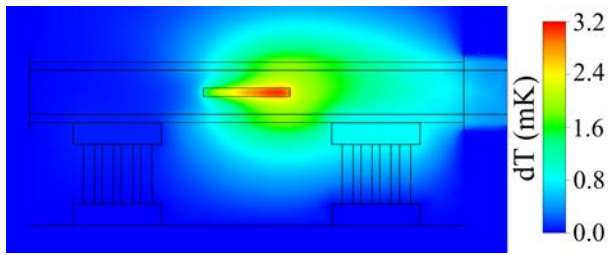


**Fig. 7.** Predicted steady state temperature increase down the centre-line of the calorimeter. The fluid flow rate was  $0.5 \mu\text{L/s}$ , the muscle heat output was  $5 \mu\text{W}$ .

the effects of the assumptions regarding heat loss to the surrounding air and heat conduction in the fluid, and the effect of the location of the temperature sensors, are best examined by using finite element methods. In addition, the use of finite element methods allows us to consider the potential advantage of locating additional sensors on the side faces of the glass tube.

Geometric models of the TEMs and the muscle calorimeter were generated in Solidworks and then imported into ANSYS CFX for analysis. Models were meshed using up to 850,000 tetrahedral elements. The calorimeters were modelled with up to three TEMs (on the bottom and two side faces) located upstream and downstream of the muscle heat-source. Fluid flow and muscle heat output were set at  $0.5 \mu\text{L/s}$  and  $5 \mu\text{W}$ , respectively. The flow was laminar as the Reynold's number was approximately 0.5. The top and bottom surfaces of the calorimeter block were held at ambient temperature, while the sides of the calorimeter were modelled as adiabatic boundaries. The fluid and thermal flow equations were solved to steady state.

An example of the steady state temperature distribution predicted by the finite element model is shown in Fig. 7. While the maximum temperature change of the muscle approached 3 mK, the temperature increase of the downstream thermopile was no more than 1 mK across all of the analyses. The temperature difference between the top and bottom substrates was extracted from the model at the upstream and downstream locations. The difference between the downstream and upstream temperature differences was then calculated, allowing the expected voltage signal to be found. A Seebeck coefficient of  $202 \mu\text{V/K}$  was assumed for the bismuth telluride thermocouples (Laird Technologies, 2013). The voltage signal was then divided by the Johnson noise to give the expected SNR of each design.

Each of the thermopiles listed in Table I was examined using this finite element modeling approach, with the results (FEM SNR) shown in table II. The general trends revealed by this analysis are similar to the analytical predictions, but have much smaller SNRs, as the analysis now takes into account heat loss into the surrounding air, and heat conduction within the fluid. For example, the analytical model gave a SNR of 4650 for a single Watronix inbM1-8-1.3-0.4 thermopile; the equivalent finite element model predicted a SNR of 1770.

In practice, the amplifiers used to measure the output of the thermopiles also inject noise into the measurement circuit. Consequently, the amplifier-limited SNR must also be considered. The nanovolt-amplifiers chosen for use in this device (EM electronics A10) provided input noise equivalent to a  $20 \Omega$  resistor, which can be considered in series with the thermopile resistance. The corresponding 'Amp-limited SNR' is shown in the final column of Table II.

TABLE II. THERMOPILE PROPERTIES

Module	# of modules per end	$\Delta T$ (mK)	$V_s$ ( $\mu\text{V}$ ) <sup>a</sup>	$V_n$ ( $\mu\text{V}$ ) <sup>b</sup>	Analytical SNR	FEM SNR	Amp-limited SNR <sup>c</sup>
Laird OT08-0203	1	0.64	0.74	0.3	4790	2000	330
	2	0.46	1.08	0.43	4720	1920	440
	3	0.36	1.24	0.52	4440	1720	470
Laird OT08-0305	1	0.46	1.06	0.43	4720	1910	430
	2	0.32	1.46	0.6	4160	1670	520
Micopelt MPC-D303	1	0.15	0.17	0.22	3000	460	60
Micopelt MPG-D651	1	0.006	0.52	5.52	2520	70	60
Watronix inbM1-4-1.3-0.4	1	0.95	1.11	0.46	4030	1670	410
Watronix inbM1-4-1.6-1.3	1	0.39	0.45	0.25	4660	1280	180
Watronix inbM1-8-1.3-0.4	1	0.76	1.77	0.7	4650	1770	630
	2	0.65	3.03	0.99	4820	2450	1170
	3	0.54	3.76	1.21	4650	2390	1330

<sup>a</sup>  $V_s$  indicates the expected signal voltage

<sup>b</sup>  $V_n$  indicates the expected Johnson noise.

<sup>c</sup> Amp-limited SNR indicates the SNR when considering both the noise-equivalent resistances of the amplifiers and the resistances of the TEMs. All devices used bismuth telluride thermocouples, which were presumed to have identical Seebeck coefficients of  $202 \mu\text{V}\cdot\text{K}^{-1}$  (Laird Technologies, 2013).

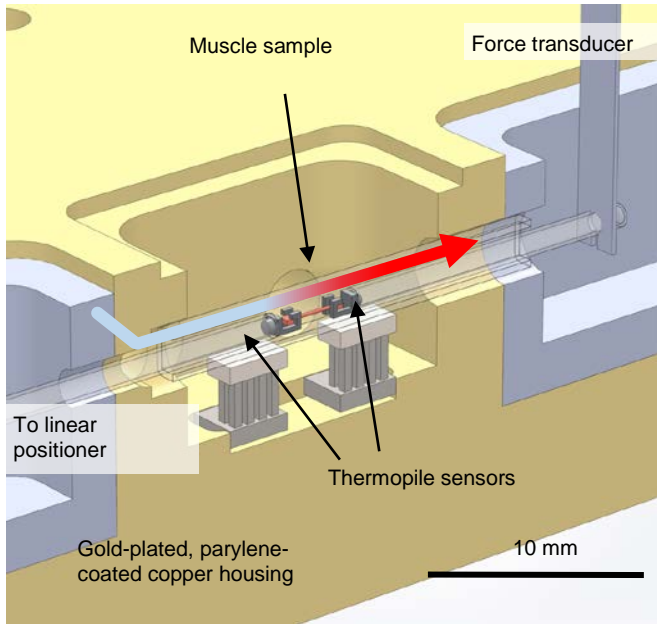


**Fig. 8.** Section view of the centre of the calorimeter measurement chamber sensor. The coloured arrow indicates the path and temperature increase of the fluid.

This analysis revealed that the Watronix inbM1-8-1.3-0.4 thermopiles provided superior performance to the other options. Even the use of a single thermopile, located at each temperature measurement point, upstream and downstream of the muscle, provides a SNR of 630, when taking into account amplifier noise. The  $2\text{ mm} \times 2\text{ mm}$  substrate dimensions are a good match to the outer dimensions of the glass tube. The use of two or three sensors at the temperature measurement positions further increases the SNR to 1170 and 1330 respectively, at the expense of construction complexity.

### III. METHODS

#### A. Muscle Calorimeter

The analyses detailed in Section II allowed us to select a design for our calorimeter that provides enhanced performance over previous devices, yet was relatively simple to construct, and robust against regular use. Our analysis had indicated that the Watronix inbM1-8-1.3-0.4 thermopiles would provide an SNR of at least 630. To minimise construction complexity, we thus chose to design a calorimeter with only a single thermopile located upstream and downstream of the muscle.

The selected thermopiles (Watronix inbM1-8-1.3-0.4) were placed 4 mm apart with their measurement junctions attached to the lower surface of a glass tube of square cross-section, as shown in Fig. 8. The reference end of the thermopiles was adhered to a parylene-coated gold-plated copper housing using ceramic-loaded epoxy adhesive.

The thermopile voltages were amplified by preamplifiers (EM Electronics A10, gain = 10000) and digitized at a rate of 50 kHz, using simultaneous-sampling 24-bit analog to digital converters (National Instruments NI 9239), and electronically filtered and down-sampled to 10 Hz bandwidth. The difference between the upstream and downstream voltages

was computed in software and divided by the flow-rate-

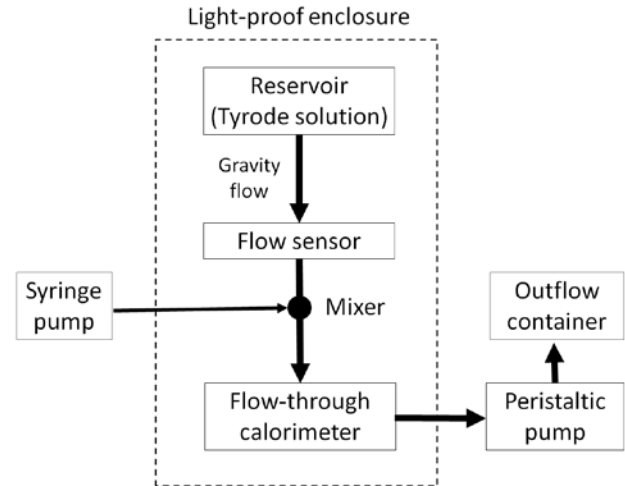


**Fig. 9.** Schematic view of the fluid flow system.

dependent sensitivity (in V/W) to provide an estimate of the muscle heat rate.

Platinum electrodes (not shown) placed at each end of the measurement chamber enabled muscle contraction via field stimulation. As in our previous devices, quartz tubes (0.7 mm OD) and platinum hooks were used to secure the muscle to a linear positioner (upstream) and interferometric force transducer (downstream). The custom-made force transducer (see [1] for details) comprised a cantilever of stainless steel (1 mm width, 8 mm length, 0.15 mm thickness). The deflection of the cantilever was measured by a laser interferometer (Keysight Technologies) to 0.31 nm resolution, providing an estimate of muscle force. This type of force transducer is robust, provides high-resolution, and does not inject heat into the calorimeter environment. All software was developed in the LabVIEW programming environment (National Instruments).

#### B. Fluid-titration and mixing system

One of the key requirements for the instrument was the ability to infuse a concentrated pharmacological agent into a flowing, oxygenated Tyrode (saline) solution. This was achieved using two synchronized pumping systems; their outflows were combined just prior to entry into the calorimeter body, in order to allow the heat of dilution to dissipate before the fluid reached the temperature sensors and muscle sample (Fig. 9.). Since the sensitivity of the calorimeter is dependent on flow rate, care was taken to ensure that the flow rate was smooth and constant.

The Tyrode solution fluid flow control system comprised a vertical linear motor (Parker-Daedel MX80L with pneumatic counterbalance (not shown)) that controlled the elevation of a heated water-jacketed oxygenation reservoir. Fluid drained from the chamber into the mixer via a flow sensor (Sensirion SLI-0430), oxygen-impervious tubing (Tygon) and a flow restrictor ( $200\text{ }\mu\text{m}$  diameter  $\times$  30 mm length). The flow rate of the Tyrode solution was measured to 16-bit resolution at a rate of 10 Hz, and transferred to a control computer by RS-422

protocol. A software-based feedback algorithm adjusted the height of the oxygenation chamber to achieve the desired fluid flow rate, in the range 0.4  $\mu\text{L/s}$  to 0.6  $\mu\text{L/s}$ .

The concentrate was delivered by a computer-controllable syringe pump (PhD Ultra, Harvard Apparatus) from a 50  $\mu\text{L}$  gas-tight syringe (Hamilton, #1705) through 200  $\mu\text{m}$  inner diameter flexible fused silica tubing (Polymicro). The concentrate typically was delivered at a rate of 20  $\text{nL/s}$  and mixed with Tyrode solution which was flowing at a rate of  $\sim 480$   $\text{nL/s}$ , thus achieving an overall flow rate of 500  $\text{nL/s}$ . Outflow from the calorimeter was aspirated together with air through a porous filter constructed of balsa wood, using a peristaltic pump (Langer Instruments BQ50-1J).

### C. Temperature control system

In order to isolate the experiment from environmental noise and to raise the experimental temperature from room temperature to 37  $^{\circ}\text{C}$ , a temperature control and isolation system was implemented, as described previously [23]. Briefly, the calorimeter measurement chamber was enclosed between temperature controlled copper blocks, and wrapped in foil-coated closed-cell foam. Thermistors were used to monitor the temperature of each block; thermoelectric heat pumps were used to direct heat in and out of the blocks, under the control of software based temperature-control algorithms.

### D. Muscle preparation and superfusate solutions

A Wistar rat was anaesthetized using isoflurane prior to cervical dislocation (as approved by The University of Auckland Animal Ethics Committee). The heart was excised and quickly plunged into a cold Tyrode solution. The aorta was immediately cannulated and the coronary vasculature was Langendorff-perfused with Tyrode solution equilibrated with 100% oxygen. A right-ventricular trabecula muscle was dissected and transferred to the infusion calorimeter containing superfusate (Tyrode solution: 130  $\text{mmol/L}$  NaCl; 6  $\text{mmol/L}$  KCl; 1.5  $\text{mmol/L}$   $\text{MgCl}_2$ ; 0.5  $\text{mmol/L}$   $\text{NaH}_2\text{PO}_4$ ; 1.5  $\text{mmol/L}$   $\text{CaCl}_2$ ; 10  $\text{mmol/L}$  HEPES; and 10  $\text{mmol/L}$  glucose with pH corrected to 7.4 using Tris). For measurements of barium-induced muscle contracture, the concentration of  $\text{CaCl}_2$  in the Tyrode solution was reduced to 0.1  $\text{mmol/L}$ . The Tyrode solution was vigorously bubbled with 100%  $\text{O}_2$ , at 41  $^{\circ}\text{C}$  and passed along the length of the muscle at a precisely-controlled rate in the range of 0.5  $\mu\text{L/s}$  to 0.55  $\mu\text{L/s}$ .

Each trabecula was electrically stimulated at 3 Hz (amplitude between 6 V and 10 V, duration from 6 ms to 10 ms) until fully recovered from dissection and an optimal calorimeter chamber temperature was achieved. Trabeculae were considered to have recovered when force production reached a steady state and reducing the stimulus voltage or stimulus duration to typical supra-threshold values (6 V, 6 ms) had no impact on the force production. Muscle volume was estimated by using a microscope graticule to estimate the length and two orthogonal diameters of the specimen.

## E. Experiments

### 1) Calorimeter Performance

The sensitivity, noise and time-response of the calorimeter were determined at an operating temperature of 37  $^{\circ}\text{C}$ . Calibration was performed by liberating a square wave of electrical power from a thin-film resistor (1  $\text{k}\Omega$ , 0402) that was soldered to a flexible circuit film and placed in the center of the measurement chamber. The difference between the thermopile voltages was determined while the Tyrode solution was passed through the calorimeter at 0.5  $\mu\text{L/s}$ , 0.52  $\mu\text{L/s}$  and 0.55  $\mu\text{L/s}$ .

The noise of the voltage signal was measured in the absence of any heat source. Ten signals (each with a period of 100 s) were recorded and their power spectral densities calculated. The power spectral densities were averaged and the RMS magnitude of the resulting signal was calculated over a 50  $\text{mHz}$  to 5  $\text{Hz}$  bandwidth. These experiments were performed with and without fluid flow at room temperature (approximately 23  $^{\circ}\text{C}$ , although the temperature was not explicitly controlled), 27  $^{\circ}\text{C}$ , and 37  $^{\circ}\text{C}$ .

The variability of the flow rate of the Tyrode solution was quantified by the amplitude spectral density of the flow rate measured over a bandwidth of 50  $\text{mHz}$  to 1  $\text{Hz}$ . The variability of flow from the syringe pump was not directly measured, but its contribution to overall flow noise is likely to be negligible.

### 2) Heat of Mixing

One of the motivations for constructing this instrument was the need to quantify the contribution of activation heat to total muscle heat production at 37  $^{\circ}\text{C}$ . ('Activation heat' is a term that refers to the energetic cost of engaging and maintaining the cellular processes that put the muscle in a state where it is able to produce force; the energetic cost of muscle force-production itself ('cross-bridge heat') sums with this to give the total heat (above resting heat) evolved by the muscle during force production.) However, before conducting these measurements, it was first necessary to explore the possible effect of the heat of dilution or mixing.

First, Tyrode solution was flowed into the calorimeter to establish a baseline value for subsequent infusions. Second, we infused, at 20  $\text{nL/s}$ , a concentrate containing a 10% solution of dimethylsulfoxide (DMSO) – a biologically-compatible solvent that is convenient for use with salt compounds. After initiating infusion, we looked for any change in the temperature signals detected in the calorimeter, which might indicate the presence of the heat of dilution. Next, we infused into the calorimeter a 10% DMSO solution containing 0.375  $\text{mmol/L}$  blebbistatin, an inhibitor of the muscle cross-bridge force production cycle [24]. After it had mixed with the Tyrode solution, the final concentration of blebbistatin was 15  $\mu\text{mol L}^{-1}$ . We recorded any consequent changes to heat production. Finally, the infusion was ceased, allowing Tyrode solution alone to flow into the measurement chamber. The duration of each intervention was 30 minutes.

### 3) Heat of Activation

Using a second muscle, we then conducted a series of measurements of muscle heat production in the absence and

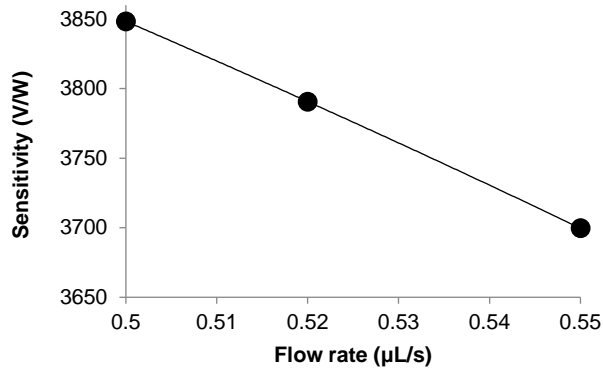


Fig. 10. Thermal sensitivity as a function of superfusate flow rate.

presence of blebbistatin. A muscle was mounted in the calorimeter and allowed to settle to steady state force during exposure to Tyrode solution. The muscle was then stretched to its optimal length  $L_o$  – the length beyond which no further active force could be developed without additional ‘resting’ (ie passive) force. Muscle heat rate was measured over a period of 60 s, as the muscle was stimulated at a rate of 5 Hz. Muscle length was shortened in 5 steps to approximately  $0.77 L_o$  – a length at which no active force was produced during a muscle twitch. Subsequently, the muscle was stretched back to  $L_o$ , and the experimental protocol was repeated during the infusion of DMSO and blebbistatin.

#### 4) Heat of Forced Contraction

We conducted a third muscle experiment to determine the total heat rate of a muscle during a chemically-initiated sustained contracture. This experiment was designed to reveal the oxidative contribution to heat release during the life-threatening condition of malignant hyperthermia [25]. This experiment was conducted at  $32^\circ\text{C}$ , to reproduce the temperature typically experienced by peripheral muscle tissue, *in vivo* [26], and to reduce the risk of the irreversible muscle damage that often ensues at body temperature [27].

First, solution containing  $35\text{ mmol/L CaCl}_2$  was supplied to the measurement chamber via the infusion syringe pump at a rate of  $20\text{ nL/s}$  to provide a calcium concentration of  $1.5\text{ mmol/L}$  when mixed with the Tyrode solution. The total heat rate and force were recorded as the muscle was stimulated at a rate of  $1\text{ Hz}$ . Once a steady state was achieved, stimulation was ceased, and the calcium solution in the syringe pump was replaced with a solution containing  $37.5\text{ mmol/L BaCl}_2$  to provide  $1.5\text{ mmol/L}$  barium concentration in the measurement chamber. The muscle force and heat production were recorded simultaneously.

## IV. RESULTS

### A. Calorimeter Performance

The calibration of the calorimeter revealed its sensitivity at a flow rate of  $0.5\text{ μL/s}$  to be  $3850\text{ V/W}$ , and to decline with increasing flow rate (Fig. 10.) The step response time of the calorimeter at this flow rate was similar to that of our previous designs: approximately 15 s.

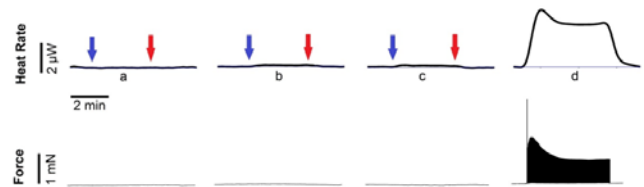


Fig. 11. Heat rate and force measurements during resting (a, b and c) and actively-contracting (d) states of a superfused muscle: a. During Tyrode infusion; b. During infusion of DMSO; c. During infusion of DMSO and Blebbistatin; d. During a typical 180 s period of muscle heat-production at a stimulus frequency of 5 Hz. Arrows denote the arrival (blue) of the infused mixture into the measurement chamber, and its exit (red).

The series resistance of the TEMs was  $2.97\text{ Ω}$  per TEM while the noise-equivalent resistance of the amplifiers was  $20\text{ Ω}$  per amplifier. Their combined equivalent Johnson noise was  $1.93\text{ nV}$ , determined over the measurement bandwidth. The recorded voltage noise at room temperature ( $23^\circ\text{C}$ ) was  $1.88\text{ nV}$  and  $1.91\text{ nV}$ , with and without fluid flow, respectively. The sensor thus operated near the limits of the expected Johnson noise at room temperature.

Controlling and increasing the operating temperature introduced additional noise, due to temperature noise injected by the temperature controllers. With fluid flow, the temperature amplitude spectral density was  $0.37\text{ μK}\cdot\text{Hz}^{-1/2}$ ,  $0.47\text{ μK}\cdot\text{Hz}^{-1/2}$  and  $1.01\text{ μK}\cdot\text{Hz}^{-1/2}$  at room temperature ( $23^\circ\text{C}$ ),  $27^\circ\text{C}$ , and  $37^\circ\text{C}$ , respectively. The corresponding power amplitude spectral density was  $2.6\text{ nW}\cdot\text{Hz}^{-1/2}$ ,  $3.3\text{ nW}\cdot\text{Hz}^{-1/2}$ , and  $7.1\text{ nW}\cdot\text{Hz}^{-1/2}$ , respectively. The expected rate of heat output of a muscle is approximately  $10\text{ μW}$  at room temperature and  $27^\circ\text{C}$ , and  $5\text{ μW}$  at  $37^\circ\text{C}$ . Consequently, the SNR over the measurement bandwidth is 1700 at room temperature, 1350 at  $27^\circ\text{C}$ , and 315 at  $37^\circ\text{C}$ .

The Tyrode solution flow control system maintained the flow rate constant to within  $0.4\text{ nL/s}$  (one standard deviation) of the set flow rate of  $0.5\text{ μL/s}$ . The time delay between the onset of infusion and the exposure of the infused solution to the muscle was approximately 10 minutes.

### B. Heat of mixing

In this experiment, the heat measurement system was nulled with the muscle at rest in the centre of the chamber (Fig 11a).

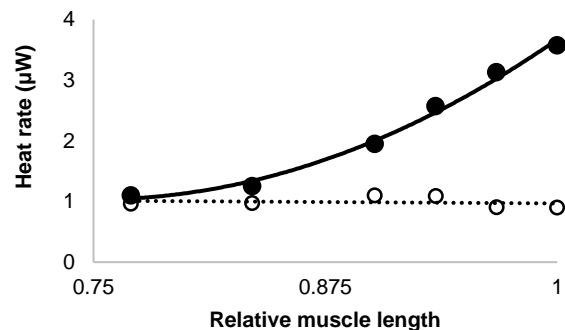
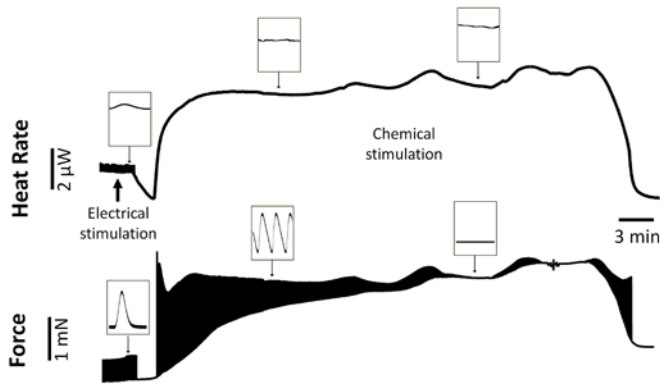


Fig. 12. Muscle active heat rate: solid circles indicate normal Tyrode infusion; open circles indicate DMSO+blebbistatin infusion.



**Fig. 13.** Muscle heat rate and force development during electrical stimulation, which is ceased prior to chemical stimulation (barium induced contracture). Insets show the heat rate and force responses during electrical stimulation, and that arose spontaneously during the development of contracture. Contracture was reversed by washing out barium at the end of the experiment.

Upon the arrival of the DMSO solution in the measurement chamber, a small increase ( $0.11 \mu\text{W}$ ) in heat rate was detected (Fig 11b). Addition of blebbistatin to the DMSO made no appreciable increase in heat rate (Fig 11c). Thus, the heat of mixing (for this experiment) was  $0.11 \mu\text{W}$ , and was accounted for in subsequent analyses. Finally, the infusion was terminated, allowing normal Tyrode solution to superfuse the muscle. The resulting muscle heat rate is shown in Fig 11d.

### C. Heat of activation

The heat rate of activation was found to be invariant with muscle length (Fig. 12) at approximately  $1 \mu\text{W}$ . The active heat rate was found to increase to approximately  $3.6 \mu\text{W}$  when this muscle was stretched to  $L_o$ . Thus, at optimal length, approximately 27 % of the energy consumed by this muscle was involved with activating the contractile machinery while the remainder of the heat was associated with producing force.

### D. Heat of forced contracture

The active heat rate during 1 Hz electrical stimulation was approximately  $2.5 \mu\text{W}$  (Fig. 13). When electrical stimulation was ceased, the heat rate began to decline back toward its “resting” level. Upon infusion of  $\text{BaCl}_2$ , the muscle heat rate increased to approximately  $8 \mu\text{W}$  as the muscle progressively transitioned into contracture. During this period the muscle began to spontaneously twitch while the resting force continuously increased, in accord with early observations [28]. After approximately 2000 s of infusion, the muscle was in complete contracture. When normalised to the muscle volume, the heat rate amounted to  $48 \text{ kW/m}^3$ . When the infusion was halted, muscle heat rate gradually declined to its resting value.

## V. DISCUSSION AND CONCLUSIONS

The sensitivity of this calorimeter exceeds (by up to 60 %) that reported for all of our previous calorimeters. This is due, in part, to our use of low-resistance thermoelectric modules and low-noise preamplifiers for temperature sensing, but may also owe to our use of copper-coated polyimide film for making electrical connection to the heat source during calibration. It is probable that with this approach the very low

thermal conductivity of the traces in the circuit prevents heat conduction from the resistor through the electrical connections, leading to more heat conducting directly into the superfusate solution, and a larger response from the downstream temperature sensor. Consequently, our calorimeter can resolve muscle heat rate to approximately  $6 \text{ nW}$ ; given a maximum measured heat rate of  $8 \mu\text{W}$ , this corresponds to a SNR of approximately 1350.

The response time of the calorimeter at this flow rate is similar to that of our previous designs ( $\sim 6 \text{ s}$ ), but could be decreased by increasing the flow rate, at the expense of sensitivity [6]. The calorimeter thus has a much lower bandwidth than the dynamics of muscle energetics and cannot fully resolve the time-course of heat-release during each twitch (Fig. 13, insets). Yet, it may be possible to deconvolve the output signal (representing the heat accumulated across several seconds) with the calorimeter impulse response function to reveal more information to a higher temporal resolution.

The oxygenation chamber can contain sufficient Tyrode solution for 24 hours of continuous experimentation. The syringe pump can contain up to  $50 \mu\text{L}$  of concentrate; at an infusion rate of  $20 \text{ nL/s}$ , this implies a total possible infusion time of 2500 s (approximately 40 min). With the use of a two-way tap, the syringe can be refilled and infusion resumed in a matter of seconds. Although the speed of the syringe pump can be changed several times per second, the time delay for the infused fluid to progress to the measurement chamber may allow significant diffusion of concentrate into the preceding or following Tyrode solution. The potential for this effect to occur has not yet been examined.

The heat of dilution in the mixing experiment was consistent, and small in comparison to the heat evolved by the muscle (Fig. 11). However, it may be necessary to determine whether this heat rate is similar for other infusions at other concentrations, on a case-by-case basis. In future, we will examine whether forced air flow could be used to improve the coupling between the mixer and the surrounding temperature-controlled air.

The direct measurements of heat of activation by this method have revealed a new finding — that the heat of activation in cardiac muscle is independent of muscle length. This finding has important implications for our interpretation of muscle heat during work production [29].

Finally, the barium experiment has provided us with an estimate of the total heat output of a muscle during chemically-induced contracture. The heat rate of  $48 \text{ W/m}^3$  is similar to that reported in other studies of cardiac tissues subjected to high-frequency electrical stimulation [30].

We are now equipped with a unique infusion calorimeter, through which we can infuse pharmacological drugs, for understanding muscle energetics under various interventions. We plan to use this device to study the effect of drug treatments on diseased cardiac and skeletal muscle tissues. We also plan to integrate this calorimeter design into a fluorescence imaging system and brightfield microscope to measure even more muscle characteristic parameters,

including intracellular calcium release and sarcomere shortening.

## REFERENCES

- [1] A. J. Taberner, J. C. Han, D. S. Loiselle, and P. M. Nielsen, "An innovative work-loop calorimeter for in vitro measurement of the mechanics and energetics of working cardiac trabeculae," *J Appl Physiol*, vol. 111, no. 6, pp. 1798-1803, 2011.
- [2] J.-C. Han, A. J. Taberner, P. M. F. Nielsen, and D. S. Loiselle, "Interventricular comparison of the energetics of contraction of trabeculae carneae isolated from the rat heart," *The Journal of Physiology*, vol. 591, no. 3, pp. 701-717, February 1 2013.
- [3] C. J. Barclay, C. Widén, and L. J. Mellors, "Initial mechanical efficiency of heat rate and force production of cardiac trabeculae carneae," *J Appl Physiol*, vol. 107, no. 3, pp. 946-951, 2009.
- [4] J. C. Han, A. J. Taberner, R. S. Kirton, P. M. Nielsen, N. P. Smith, and D. S. Loiselle, "A unique micromechanocalorimeter for simultaneous measurement of heat rate and force production of cardiac trabeculae carneae," *J Appl Physiol*, vol. 107, no. 3, pp. 946-951, 2009.
- [5] D. S. Loiselle, C. M. Johnston, J. C. Han, P. M. Nielsen, and A. J. Taberner, "Muscle heat: a window into the thermodynamics of a molecular machine," *Am J Physiol Heart Circ Physiol*, vol. 310, no. 3, pp. H311-25, Feb 1 2016.
- [6] A. J. Taberner, I. W. Hunter, R. S. Kirton, P. M. F. Nielsen, and D. S. Loiselle, "Characterization of a flow-through microcalorimeter for measuring the heat production of cardiac trabeculae," *Review of Scientific Instruments*, Journal paper vol. 76, no. 10, pp. 104902-104908, October 10 2005.
- [7] J. Daut and G. Elzinga, "Heat production of quiescent ventricular trabeculae isolated from guinea-pig heart," *Journal of Physiology*, vol. 398, pp. 259-275, 1988.
- [8] A. Taberner, T. Pham, J.-C. Han, R. Uddin, and D. Loiselle, "A flow-through infusion calorimeter for measuring muscle energetics during pharmacological interventions," in *2017 IEEE International Instrumentation and Measurement Technology Conference Turin, Italy, 2017: IEEE*.
- [9] C. M. Johnston, J. C. Han, B. P. Ruddy, P. M. Nielsen, and A. J. Taberner, "A high-resolution thermoelectric module-based calorimeter for measuring the energetics of isolated ventricular trabeculae at body temperature," *Am J Physiol Heart Circ Physiol*, vol. 309, no. 2, pp. H318-24, Jul 15 2015.
- [10] V. Baier *et al.*, "Highly sensitive thermopile heat power sensor for micro-fluid calorimetry of biochemical processes," *Sensors and Actuators A: Physical*, vol. 123, pp. 354-359, 2005/09/23/ 2005.
- [11] A. Bourque-Viens, V. Aimez, A. J. Taberner, P. M. F. Nielsen, and P. G. Charette, "Modelling and experimental validation of thin-film effects in thermopile-based microscale calorimeters," *Sensors and Actuators A-Physical*, Journal paper vol. 150, no. 2, pp. 199-206, 2009.
- [12] C. M. Johnston, P. M. F. Nielsen, I. W. Hunter, and A. J. Taberner, "A vapor pressure thermometer for use in muscle microcalorimetry," in *Annual International Conference of the IEEE Engineering in Medicine and Biology Society, EMBC, 2011* 2011, pp. 520-523.
- [13] C. M. Johnston, P. M. F. Nielsen, I. W. Hunter, and A. Taberner, "Vapor pressure thermometry at room temperature," in *2017 IEEE International Instrumentation and Measurement Technology Conference Turin, Italy, 2017: IEEE*.
- [14] H. Y. Leung, D. M. Budgett, A. J. Taberner, and A. P. Hu, "Power loss measurement of implantable wireless power transfer components using a Peltier device balance calorimeter," *Measurement Science and Technology*, vol. 25, no. 9, p. 095010, 2014.
- [15] D. F. Frost and D. A. Howey, "High-Speed Peltier Calorimeter for the Calibration of High-Bandwidth Power Measurement Equipment," *IEEE Transactions on Instrumentation and Measurement*, vol. 65, no. 1, pp. 155-163, 2016.
- [16] S. J. McEuen and Massachusetts Institute of Technology. Dept. of Mechanical Engineering., "The design and characterization of a microcalorimeter to aid drug discovery," Thesis S.M. --Massachusetts Institute of Technology Dept. of Mechanical Engineering 2008., 2008.
- [17] O. Braissant *et al.*, "Isothermal microcalorimetry accurately detects bacteria, tumorous microtissues, and parasitic worms in a label-free well-plate assay," *Biotechnology Journal*, vol. 10, no. 3, pp. 460-468, 2015.
- [18] S. Lineykin and S. Ben-Yaakov, "Modeling and Analysis of Thermoelectric Modules," *IEEE Transactions on Industry Applications*, vol. 43, no. 2, pp. 505-512, 2007.
- [19] Z. Ouyang and D. Li, "Modelling of segmented high-performance thermoelectric generators with effects of thermal radiation, electrical and thermal contact resistances," *Scientific Reports*, Article vol. 6, p. 24123, 04/07/online 2016.
- [20] B. Yang, H. Ahuja, and T. N. Tran, "Review Article: Thermoelectric Technology Assessment: Application to Air Conditioning and Refrigeration," *HVAC&R Research*, vol. 14, no. 5, pp. 635-653, 2008/09/01 2008.
- [21] H. Kraus, "Superconductive bolometers and calorimeters," *Superconductor Science and Technology*, vol. 9, no. 10, p. 827, 1996.
- [22] W. Franzen, "Nonisothermal Superconducting Bolometer - Theory of Operation," (in English), *Journal of the Optical Society of America*, vol. 53, no. 5, pp. 596-&, 1963.
- [23] A. J. Taberner *et al.*, "Measuring the mechanical efficiency of a working cardiac muscle sample at body temperature using a flow-through calorimeter," in *37th Annual International Conference of the IEEE Engineering in Medicine and Biology Society, Milan, Italy, 2015*.
- [24] C. J. Barclay, "Quantifying Ca(2+) release and inactivation of Ca(2+) release in fast- and slow-twitch muscles," *The Journal of Physiology*, vol. 590, no. Pt 23, pp. 6199-6212, 2012 2012.
- [25] H. Rosenberg, N. Pollock, A. Schiemann, T. Bulger, and K. Stowell, "Malignant hyperthermia: a review," *Orphanet Journal of Rare Diseases*, journal article vol. 10, no. 1, p. 93, August 04 2015.
- [26] K. Belani *et al.*, "Leg heat content continues to decrease during the core temperature plateau in humans anesthetized with isoflurane," (in eng), *Anesthesiology*, vol. 78, no. 5, pp. 856-63, May 1993.
- [27] G. J. Galloway and M. A. Denborough, "Suxamethonium chloride and malignant hyperthermia," *BJA: British Journal of Anaesthesia*, vol. 58, no. 4, pp. 447-450, 1986.
- [28] D. F. Munch, H. T. Comer, and J. M. Downey, "Barium contracture: a model for systole," *American Journal of Physiology - Heart and Circulatory Physiology*, vol. 239, no. 3, pp. H438-H442, 1980.
- [29] T. Pham *et al.*, "Does the intercept of the heat-stress relation provide an accurate estimate of cardiac activation heat?," *The Journal of Physiology*, 2017.
- [30] C. M. Johnston, J.-C. Han, D. S. Loiselle, P. M. F. Nielsen, and A. J. Taberner, "Cardiac activation heat remains inversely dependent on temperature over the range 27–37°C," *American Journal of Physiology - Heart and Circulatory Physiology*, vol. 310, no. 11, pp. H1512-H1519, 2016-06-01 2016.